AGU ADVANCING EARTH AND SPACE SCIENCE

Geophysical Research Letters

RESEARCH LETTER
10.1029/2020GL092208

Diffuse Auroral Electron Scattering by Electrostatic Electron Cyclotron Harmonic Waves in the Dayside Magnetosphere

Yuequn Lou[1], Xing Cao[1], Binbin Ni[1,2], Weichao Tu[3], Xudong Gu[1], Song Fu[1], Zheng Xiang[1], and Xin Ma[1]

[1]Department of Space Physics, School of Electronic Information, Wuhan University, Wuhan, China, [2]CAS Center for Excellence in Comparative Planetology, Hefei, China, [3]Department of Physics and Astronomy, West Virginia University, Morgantown, WV, USA

Key Points:

- We quantitatively evaluate the scattering effect of dayside electron cyclotron harmonic (ECH) waves on diffuse auroral electrons
- ECH waves can efficiently pitch angle scatter electrons at energies from 300 eV to 10 keV on timescales from a few hours to ~1 day
- Scattering of ~300 eV–2 keV electrons can even approach the strong diffusion limit, resulting in an almost fully filled loss cone

Supporting Information:

- Supporting Information S1

Correspondence to:
X. Cao and B. Ni,
cxing@whu.edu.cn;
bbni@whu.edu.cn

Citation:
Lou, Y., Cao, X., Ni, B., Tu, W., Gu, X., Fu, S., et al. (2021). Diffuse auroral electron scattering by electrostatic electron cyclotron harmonic waves in the dayside magnetosphere. *Geophysical Research Letters*, *48*, e2020GL092208. https://doi.org/10.1029/2020GL092208

Received 19 DEC 2020
Accepted 16 FEB 2021

Abstract Although electrostatic electron cyclotron harmonic (ECH) waves are frequently observed in the dayside magnetosphere, their effects on the formation of dayside diffuse aurora remain poorly understood. In this study, we quantitatively evaluate the efficiency of dayside ECH wave scattering in producing the electron diffuse aurora precipitation during a typical ECH wave event by calculating the quasi-linear bounce-averaged scattering rates. We find that dayside ECH waves can efficiently pitch angle scatter diffuse auroral electrons on timescales of a few hours to ~1 day over a broad range of electron energy and equatorial pitch angle α_{eq}, that is, from ~300 eV to 10 keV with α_{eq} from the loss cone to 45°. Especially for ~300 eV–2 keV electrons, the scattering rates can even approach the strong diffusion limit, resulting in an almost fully filled loss cone. Our results confirm the significant role of ECH waves in driving the dayside diffuse aurora.

Plain Language Summary Electrostatic electron cyclotron harmonic (ECH) waves are electrostatic emissions observed between the harmonics of electron cyclotron frequency with wave normal near perpendicular to the ambient magnetic field. ECH waves are known to be excited by the loss cone instability of hot electron velocity distribution. In this study, we perform a detailed survey of a typical dayside ECH wave event observed by MMS1 spacecraft on 11 Dec 2015. Using a realistic magnetic field model and a latitudinal varying wave normal angle model based on well-fitted electron velocity distribution, we calculate the quasi-linear bounce-averaged scattering rates of electrons. Our results demonstrate that ECH waves can efficiently pitch angle scatter hundreds of eV to tens of keV electrons, which are the source of diffuse aurora. ECH wave induced scattering of ~300 eV to 2 keV electrons at low pitch angles can even approach the strong diffusion limit, resulting in an almost fully filled loss cone. These electrons can be subsequently precipitated into the atmosphere and collide with neutral molecule, forming the dayside diffuse aurora. Our results demonstrate that ECH waves play an important role in the dayside diffuse auroral precipitation.

1. Introduction

The diffuse aurora is a semi-permanent phenomenon in the Earth's polar ionosphere and acts as an important linkage for the magnetosphere-ionosphere coupling. As a predominant source of particle precipitation into the high latitude region, the diffuse aurora composes 71% of the precipitating energy fluxes during high solar wind driving conditions and 84% of that during low solar wind driving conditions (Newell et al., 2009). Satellite observations show that the averaged energy flux of the precipitating electrons is much larger than that of the precipitating ions (e.g., Hardy et al., 1985; Newell et al., 2009), indicating that electron precipitation plays a dominant role in driving the diffuse aurora activity.

It has been recognized that the plasma sheet electrons at energies of hundreds of eV to ~10 keV are the major source population for the electron diffuse auroral precipitation (Lui et al., 1977; Meng et al., 1979). Via resonant interactions with plasma waves, these electrons could be pitch angle scattered into the atmospheric loss cone, resulting in the generation of diffuse aurora (Frey et al., 2019; Lui et al., 1977; Meng et al., 1979; Ni et al., 2016; Thorne et al., 2010; Zhang et al., 2019). Two different plasma waves can resonate with electrons in this energy range, including whistler mode chorus waves and electrostatic electron cyclotron harmonic

(ECH) waves. Both chorus waves and ECH waves have been proposed to contribute significantly to the nightside electron diffuse aurora (Horne et al., 2003; Meredith et al., 2009; Ni et al., 2008, 2011a; Thorne et al., 2010). While chorus wave induced scattering tends to dominantly drive the most intense nightside electron diffuse aurora in the inner magnetosphere at $L < \sim 8$ (Li et al., 2009a, 2011; Ni, Thorne, et al., 2011; Thorne et al., 2010), ECH waves are the major contributor to the nightside electron diffuse aurora in the outer magnetosphere at $L > 8$ (Liang et al., 2011; Ni et al., 2011b, 2012; Zhang et al., 2015). In addition, time domain structures and kinetic Alfven waves have been proposed to be responsible for diffuse aurora electron precipitation on the nightside (Chaston et al., 2015, 2018; Ma et al., 2016; Mozer et al., 2015).

The dayside diffuse aurora activity is relatively weaker compared to the nightside diffuse aurora and typically occurs in the dawn magnetic local time (MLT) sector (Han et al., 2015; Newell et al., 2009; Petrinec et al., 1999). However, the dayside diffuse aurora activity can be very strong occasionally (Han et al., 2017; Hu et al., 2012) and its effects on the dayside magnetosphere-ionosphere coupling can be significant. The dayside aurora is caused by the precipitation loss of plasma sheet electrons which drift azimuthally after being injected from the midnight sector (Sandholt et al., 2002). Pitch angle scattering by dayside chorus is proposed to be an important driver of the dayside diffuse aurora (e.g., Ni et al., 2014; Nishimura et al., 2013; Shi et al., 2012), due to the persistence of chorus waves in the dayside magnetosphere (Li et al., 2009a, 2011). In addition to chorus waves, recent statistical studies (e.g., Liu et al., 2020; Lou et al., 2018; Ni et al., 2017, 2011b; Zhang et al., 2014) have shown that ECH waves can be frequently observed in the dawn MLT sector throughout the outer magnetosphere, with an averaged wave amplitude of >0.1 mV/m. However, to the best of our knowledge, the efficiency of dayside ECH waves in producing electron diffuse auroral precipitation has not been quantitatively evaluated.

To improve the current understanding of the origin of dayside diffuse aurora, in this study we perform a detailed analysis of a typical dayside ECH wave event in the outer magnetosphere based on observations from the Magnetospheric Multiscale (MMS) spacecraft. By calculating the quasi-linear bounce-averaged pitch angle scattering rates using a realistic magnetic field model, we find that dayside ECH wave induced scattering can cause efficient precipitation loss of ~300 eV–10 keV electrons on timescales from a few hours to ~1 day, thereby demonstrating that ECH waves are an important driver of the dayside diffuse aurora in the outer magnetosphere.

2. Instrumentation and Event Overview

In the present study, we use the electric field, magnetic field, and particle observations from suites onboard the MMS spacecraft (Burch et al., 2016). The number density and electron fluxes are provided by Fast Plasma Investigator (FPI; Pollock et al., 2016) with energies ranging from 10 eV to ~30 keV. The magnetic field strength is measured by the fluxgate magnetometer (Russell et al., 2016). The information of electric and magnetic field wave power is obtained from the electric double probe (Ergun et al., 2016; Lindqvist et al., 2016) and the digital signal processor from the FIELDS suites (Torbert et al., 2016), respectively.

To estimate the effect of dayside ECH waves on the generation of the diffuse aurora, we perform a detailed analysis of a high-latitude ECH wave event in the dayside outer magnetosphere observed by the MMS1 spacecraft on December 11, 2015 during 22:00–23:40 UT. An overview of this ECH wave event is shown in Figure 1. Figures 1a and 1b display electron flux as a function of energy and time, and the electron and ion number densities versus time, respectively. These two plots provide useful information of the satellite position relative to the magnetopause. Specifically, high number density and high level of <1 keV electron flux indicate that the spacecraft is outside the magnetopause and vice versa. Therefore, the spacecraft traveled back and forth continuously across the magnetopause during this time period. The ECH emission during the event is then identified based on undisturbed magnetic field (Figure 1c) and enhanced electric field (Figure 1d) power spectral densities combined with harmonic structure with respect to local electron gyrofrequency. We also find that the ECH waves disappear when the spacecraft is in the magnetosheath, indicating that ECH waves can be used as a supplementary proxy in determining the location of the magnetopause. Considering the wave strength and satellite position, we choose the gray-shaded period at 22:50–22:53 UT for further analysis. Figures 1e–1g show the spectral densities of the first three harmonic bands of ECH waves during the selected time interval (thin color-coded curves) and their mean profiles (thick blue

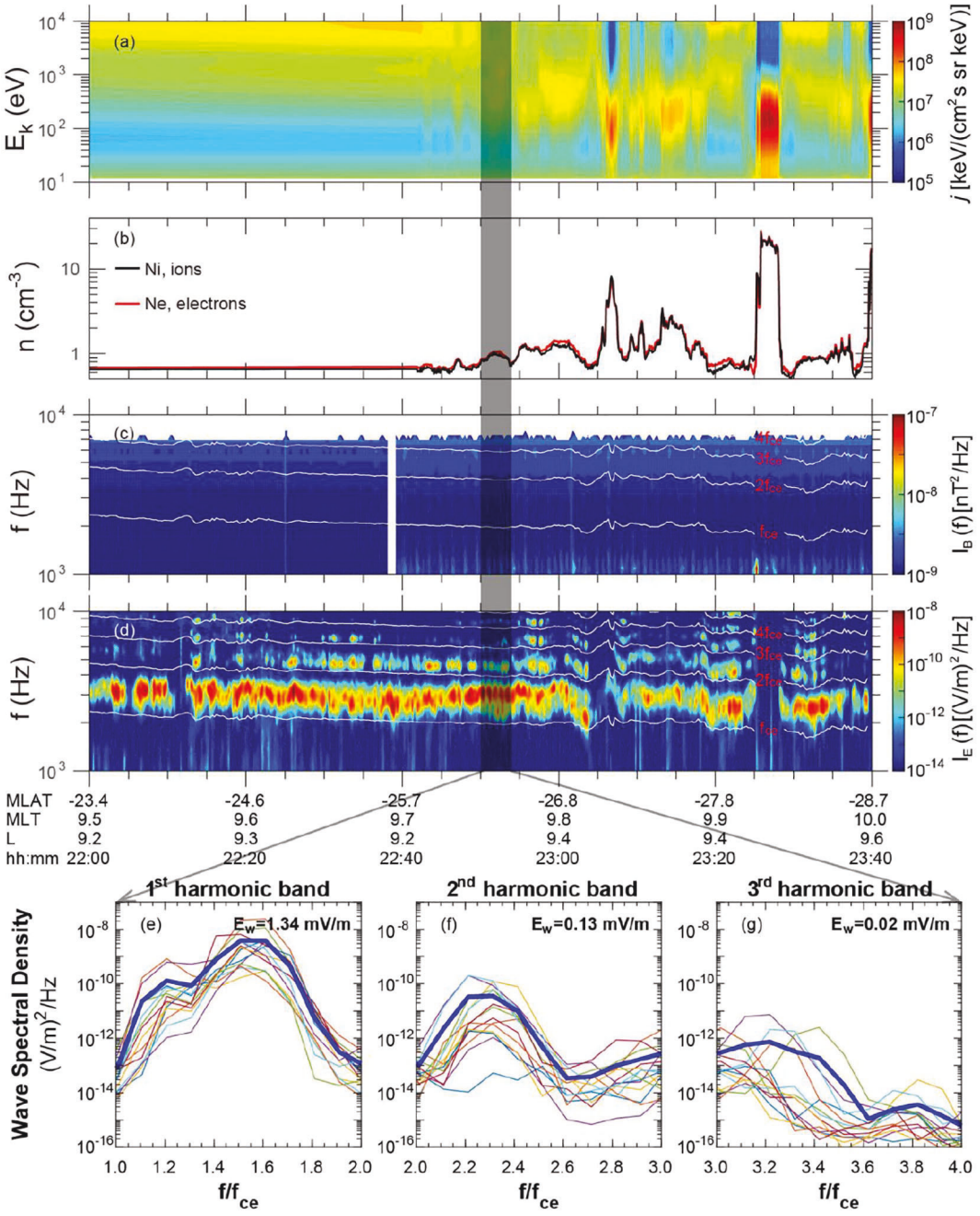

Figure 1. Overview of dayside ECH wave observed by MMS1 on December 11, 2015. (a) Electron flux as a function of energy. (b) Electron and ion number densities. (c) Magnetic field and (d) electric field power spectral densities. White lines indicate f_{ce}, $2f_{ce}$, $3f_{ce}$, $4f_{ce}$, respectively. (e–g) (from left to right) Electric field spectral densities during the gray-shaded period and the mean profile (thick blue lines) of first three harmonic band ECH waves, respectively.

curves), respectively. It is demonstrated that the wave strength of the first harmonic band is dominant in this event, which therefore would prevail in the resonant scattering of electrons by this ECH wave event. After removing the background noise, the averaged wave amplitude of the first harmonic band ECH waves during this time period is ~1.34 mV/m.

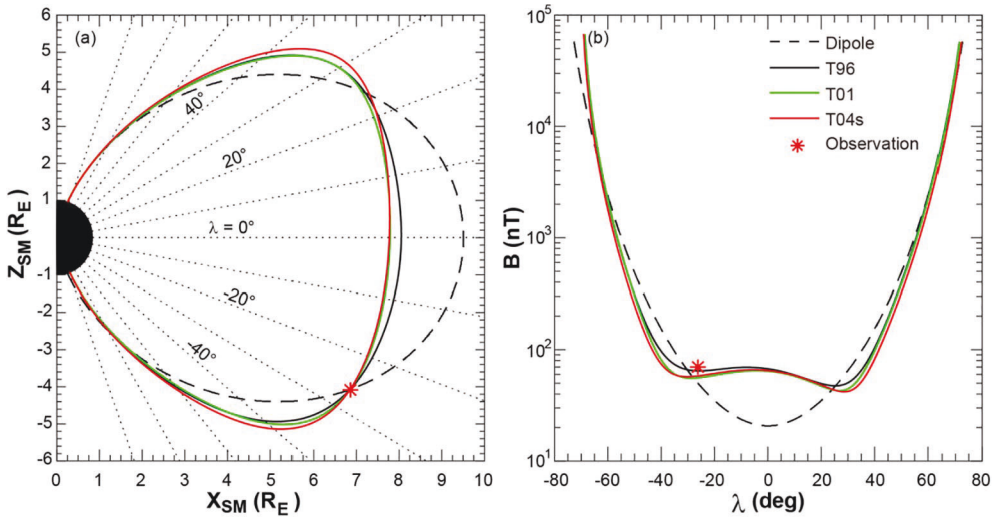

Figure 2. (a) Modeled magnetic field configuration in the SM X-Z plane along the field line traced from the MMS1 location and (b) corresponding field intensity as a function of magnetic latitude for dipole (dashed curves) and three indicated Tsyganenko (solid curves) models. The asterisks in Figures 2a and 2b correspond to the MMS1 location and observed magnetic field intensity, respectively.

3. Methods

3.1. Magnetic Field Models

It is well known that the background magnetic field topology has a strong influence on the resonant interactions between plasma waves and magnetospheric particles (e.g., Cao et al., 2016; Orlova & Shprits, 2010). In Figure 2a, we illustrate the magnetic field line configuration in the SM coordinate traced from the MMS1 location (marked by the asterisk) at 22:51 UT during the event. While the dashed curve corresponds to the dipole field, the color-coded solid curves correspond to three different Tsyganenko models (T96, T01, and T04S; Tsyganenko, 2002; Tsyganenko & Sitnov, 2005; Tsyganenko & Stern, 1996). The corresponding field intensities as a function of magnetic latitude are illustrated in Figure 2b. It is clearly shown that compared to the dipole model, the field lines for the Tsyganenko models are significantly compressed and the field intensity is much stronger near the equatorial region. In addition, two minima in field intensity can be found at high latitudes in the southern and northern hemispheres. Such a type of magnetic field topology in the dayside magnetosphere is called Shabansky orbit (Shabansky, 1971). We can see that this ECH emission is observed near the local minimum of the magnetic field intensity in the southern hemisphere, where waves tend to be excited more easily (Ashour-Abdalla & Kennel, 1978; Horne et al., 2003). Figure 2 shows that the magnetic field intensity of the T96 model is closer to spacecraft measurement than the T01 and T04S models. Thus, in this study, we use the T96 model in the quantification of ECH wave-induced scattering of diffuse auroral electrons. Based on the T96 model, we can obtain the pitch angle of loss cone $\alpha_{LC} = 1.87°$ at the magnetic equator.

3.2. ECH Wave Model

In this study, we solve the hot plasma dispersion relation of ECH waves using the WHAMP code (Ronnmark, 1982), which is applicable for both electrostatic and electromagnetic waves in a homogeneous magnetized multicomponent plasma with Maxwellian velocity distributions. As an input of the WHAMP code, the phase space density (PSD) of particles is expressed by a sum of components with the subtracted Maxwellian distribution. Each component is specified by particle species characterized by mass, density (n^j), thermal velocity (V_{th}^j), drift velocity along the magnetic field (v_{dr}^j), temperature anisotropy (α_1^j), depth of the loss cone (Δ^j), and size of the loss cone (α_2^j) with the form of Ronnmark (1982):

Table 1
Nine Electron Components Used to Fit the Measured Electron Velocity Distribution During 22:50–22:53 UT by Summation of Subtracted Maxwellian Distributions With Drift Velocity

Component	v_d (m/s)	V_{th} (eV)	α_1	Ne (m^{-3})	Δ	α_2
1	0	1	1	5.0×10^5	1.0	0.0
2	0	8.6	8.6	3.0×10^5	1.0	0.0
3	4.3×10^6	13	0.69	1.15×10^4	1.0	0.0
4	-4.3×10^6	13	0.69	1.15×10^4	1.0	0.0
5	0	155	0.32	2.97×10^5	0.75	0.30
6	0	323	0.59	2.87×10^5	0.30	0.19
7	0	800	1.20	1.77×10^5	0.58	0.22
8	0	2,900	1.21	5.17×10^4	0.66	0.12
9	0	6,200	1.08	5.74×10^4	0.85	0.27

$$f\left(v_\perp, v_\parallel\right) = \sum_{j=1}^{m} \frac{n^j}{\left(\sqrt{\pi} V_{th}^j\right)^3} \exp^{-\left(\frac{v_\parallel}{V_{th}^j} - v_{dr}^j\right)^2} \cdot \left\{ \frac{\Delta^j}{\alpha_1^j} \exp\left(-\frac{v_\perp^2}{\alpha_1^j V_{th}^{j2}}\right) + \frac{1-\Delta^j}{\alpha_1^j - \alpha_2^j} \left[\exp\left(-\frac{v_\perp^2}{\alpha_1^j V_{th}^{j2}}\right) - \exp\left(-\frac{v_\perp^2}{\alpha_2^j V_{th}^{j2}}\right) \right] \right\} \quad (1)$$

We fit the averaged electron PSD during 22:50–22:53 UT at energies from ~30 eV to ~26 keV by summing up nine components with a subtracted Maxwellian distribution. The fitting parameters of each component are listed in Table 1. Figure 3a illustrates the observed (dashed curves) and modeled (solid curves) PSD at different electron local pitch angles and energies, while Figure 3b illustrates the comparison between them in ($v_\parallel$, $v_\perp$) space. The electron PSD exhibits a field-aligned distribution at low energies and gradually becomes anisotropic at high energies. It is clearly shown in Figures 3a and 3b that our fitting results of electron PSD match the satellite observations very well. In Figure 3c, we show the effective pitch angle anisotropy $A = \frac{\int_0^\infty v_\perp dv_\perp \left(v_\parallel \frac{\partial f}{\partial v_\perp} - v_\perp \frac{\partial f}{\partial v_\parallel} \right) \frac{v_\perp}{v_\parallel}}{2 \int_0^\infty f v_\perp dv_\perp}$ (Kennel & Petschek, 1966; Li et al., 2009b) as a function of electron parallel velocity using the modeled PSD distribution. For a velocity distribution that is a product of Maxwellians, the anisotropy can be reduced to $A = T_\perp/T_\parallel - 1$, where $T_\perp$ and $T_\parallel$ are the perpendicular and parallel temperatures, respectively.

Based on the modeled electron PSD distribution and the ambient magnetic field intensity, we solve the hot plasma dispersion relation of ECH waves (Figure S1 in the supporting information) and subsequently quantify the scattering effects of ECH waves on diffuse auroral electrons by calculating the quasi-linear scattering rates. It is noted that calculation of bounce-averaged scattering rates requires the information of wave normal angle distribution along the magnetic field line, which however cannot be directly obtained from the satellite observations. Following Ni et al. (2011a), we assume that ECH waves are confined within

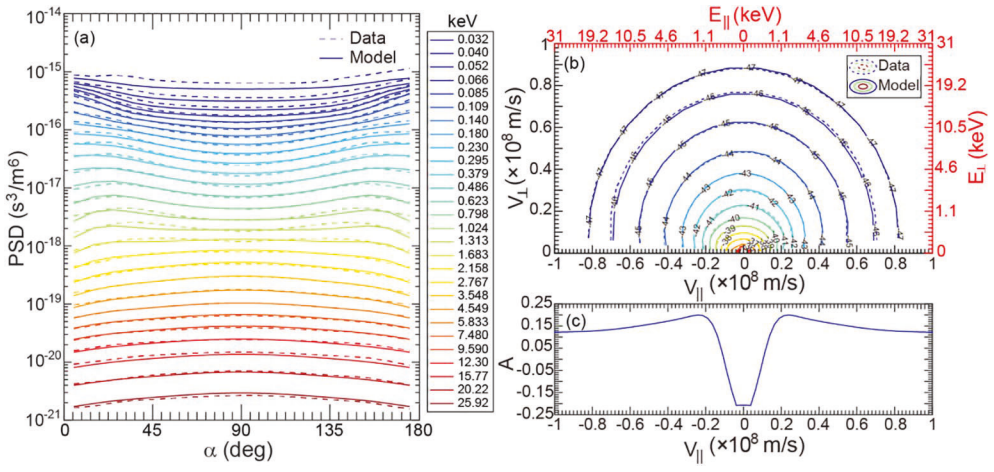

Figure 3. (a) Averaged electron phase space density (PSD) in (α, E) space during 22:50–22:53 UT. (b) Contours of the electron PSD in ln(s^3/m^6) in electron velocity ($v_\parallel$, $v_\perp$) space (or in kinetic energy ($E_\parallel$, $E_\perp$) space marked by the red axis). The dashed curves exhibit the observations from FPI instrument on the MMS1 and the solid curves show the fitted electron PSD using a multi-component loss cone distribution model. (c) Electron anisotropy as a function of parallel electron velocity.

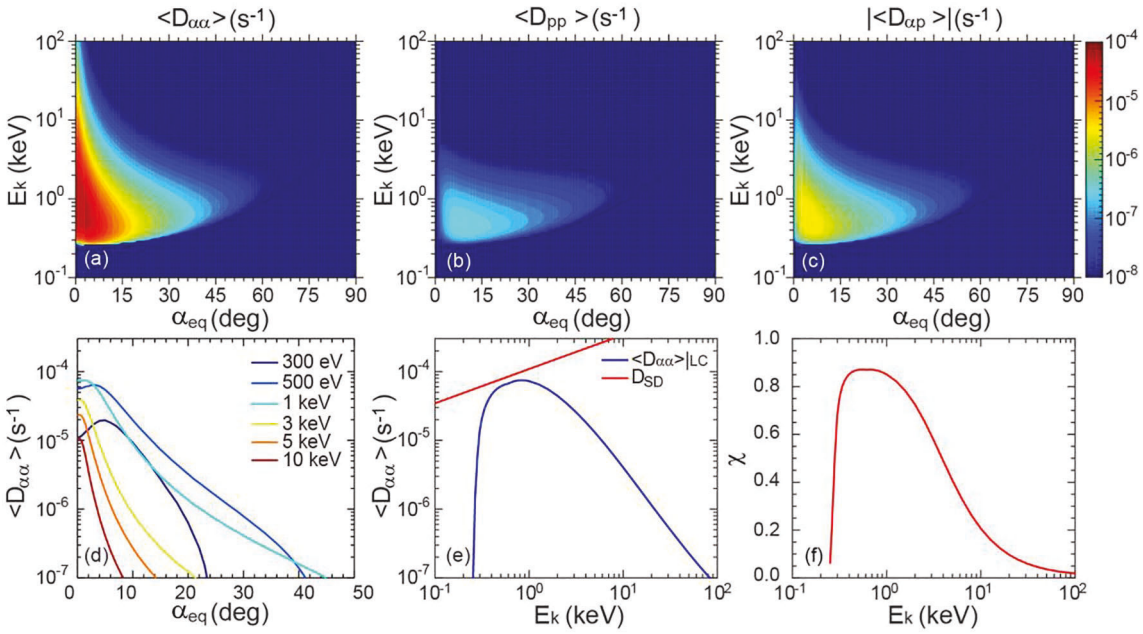

Figure 4. (a–c) (from left to right) 2-D plots of electron bounce-averaged pitch diffusion rates (<$D_{\alpha\alpha}$>), momentum diffusion rates (<D_{pp}>), and cross diffusion rates (|<$D_{\alpha p}$>|) as a function of equatorial pitch angle and electron kinetic energy for ECH waves. (d) Bounced-averaged pitch angle diffusion rates as a function of equatorial pitch angle at six specific electron energies. (e) Bounce-averaged pitch angle diffusion rates at the loss cone $D_{\alpha\alpha}$ $|_{LC}$ (blue line) and the strong diffusion rates D_{SD} (red line) as a function of electron kinetic energy. (f) Loss cone filling index χ as a function of electron kinetic energy.

±3° of the wave source region, with specific latitudinal range for each wave frequency varying with the wave normal angle of peak growth rate. More details about this wave normal angle model and the process of calculating bounce-averaged scattering rates can be referred to the supporting information.

4. Diffuse Auroral Electron Scattering by Dayside ECH Waves

Using the T96 magnetic field model and the latitude-dependent wave model, we calculate the overall quasi-linear bounce-averaged diffusion rates of electrons following previous studies (e.g., Ni et al., 2011a, 2012). Since the wave power of the first harmonic band dominates over other harmonic bands in the selected ECH wave event, we focus on the first harmonic band. We adopt wave frequency spectrum from observation which consists of nine frequencies from $1.11f_{ce}$ to $1.91f_{ce}$ with an increment of about $0.1f_{ce}$. Contributions from cyclotron resonances (from $N = -10$ to $N = 10$) and Landau resonance ($N = 0$) are included. We also assume that the power spectral densities of ECH waves and the ambient electron density remain constant along the magnetic field line.

In Figures 4a–4c, we illustrate the 2-D plots of electron bounce-averaged scattering rates as a function of electron kinetic energy E_k and equatorial pitch angle α_{eq} due to ECH waves. From Figures 4a–4c, we show the pitch angle, momentum, and mixed scattering rates, respectively. It is shown that mixed scattering rates and momentum scattering rates are much smaller than pitch angle scattering rates, which suggests that ECH waves cannot effectively accelerate electrons. ECH waves can pitch angle scatter diffuse auroral electrons over a broad range of both electron energy and equatorial pitch angle, namely, from ~300 eV to 100 keV with α_{eq} from the bounce loss cone to 45°. The largest scattering rates are generally found at pitch angles close to the loss cone and decrease significantly as α_{eq} increases, regardless of electron energy. This will result in the precipitation loss of low pitch angle electrons and the formation of the pancake distribution, which is consistent with previous studies (Horne & Thorne, 2000; Horne et al., 2003; Ni et al., 2011a; Tao et al., 2011). ECH waves can efficiently pitch angle scatter ~300 eV to 10 keV electrons at low α_{eq} at a rate of $>10^{-5}$ s^{-1}, while the pitch angle scattering of >10 keV is much weaker and occurs over a narrower range of α_{eq}. The most efficient scattering of electrons is found at energies ranging from ~400 eV to 2 keV with timescales of a few hours. We further illustrate in Figure 4d the line plots of electron bounce-averaged

pitch angle scattering rates as a function of electron equatorial pitch angle for six indicated electron energies. Except at very low pitch angles, the pitch angle scattering efficiency generally becomes weaker as the pitch angle increases. In addition, both the resonant pitch angle coverage and maximum scattering rates first increase and then decrease with increasing electron energy.

In Figure 4e, we present the bounce-averaged pitch angle scattering rates at the bounce loss cone $D_{\alpha\alpha}\,|_{\mathrm{LC}}$ (blue line) as a function of electron kinetic energy. The strong diffusion rate D_{SD}, which is shown as the red line, is given by (Cao et al., 2016; Kennel, 1969; Ni et al., 2012):

$$D_{\mathrm{SD}} = \frac{2\left(\alpha_{\mathrm{LC}}\right)^2}{\tau_B} \tag{2}$$

where α_{LC} is the loss cone angle at the magnetic equator, $\tau_B = \frac{2}{v}\int_{\lambda_{m,s}}^{\lambda_{m,n}} \sec\alpha \sqrt{r^2 + \left(\frac{\partial r}{\partial \lambda}\right)^2}\, d\lambda$ is the bounce period of particles. Figure 4e shows that pitch angle scattering rate at the loss cone first increases and then decreases with increasing electron energy, which can approach the strong diffusion limit at energies from 400 eV to 1 keV. This suggests that these electrons will be rapidly scattered into the loss cone for precipitation loss with timescales comparable to or less than the bounce period.

Once the bounce-averaged pitch angle scattering rates at the loss cone and strong diffusion rate are available, we can further estimate the loss cone filling index, which indicates the efficiency of ECH wave-induced electron precipitation loss, using the following equation (Cao et al., 2016; Kennel & Petschek, 1966; Ni et al., 2012, 2015):

$$\chi\left(E_k\right) = \frac{2\int_0^1 I_0\left[Z_0\left(E_k\right)\tau\right]\cdot\tau\cdot d\tau}{I_0\left[Z_0\left(E_k\right)\right]} \tag{3}$$

where $Z_0 = \left[D_{\mathrm{SD}} / \left\langle D_{\alpha\alpha}\right\rangle|_{\mathrm{LC}}\right]^{1/2}$, and I_0 is the modified Bessel function of the first kind, and τ is an integral variable. The results of loss cone filling index as a function of electron energy are shown in Figure 4f. The loss cone filling index with a value of < 0.2, ~ 0.2–0.8, and > 0.8 corresponds to an almost empty, partially filled, and fully filled loss cone, respectively.

We can clearly see that the loss cone filling index increases sharply at low energies and then decrease substantially at higher energies. For ~300 eV to 2 keV electrons, the corresponding loss cone filling index is > ~0.8, indicating that the ECH wave induced scattering of these electrons is strong enough to almost fully fill the loss cone. It is also noted that although pitch angle scattering of 2–10 keV electrons is weaker than that of 300 eV to 2 keV electrons, these electrons can be also effectively scattered by ECH waves with a partially filled loss cone. Following previous studies (e.g., Ma et al., 2020), we calculate the precipitating fluxes of electrons due to ECH waves, as shown in Figure S2. It is illustrated that the precipitating fluxes of 300 eV to 2 keV are comparable to the observed fluxes outside the loss cone. Our results confirm that ECH waves in the outer magnetosphere are capable of causing sufficient scattering of electrons into the auroral ionosphere to account for the occurrence of dayside diffuse aurora.

5. Summary and Discussion

In this study, we perform a detailed quantitative investigation of a typical dayside ECH wave event in the outer magnetosphere observed by MMS spacecraft. By calculating the quasi-linear bounce-averaged scattering rates using a realistic magnetic field model, we evaluate the efficiency of dayside ECH waves in the precipitation loss of diffuse auroral electrons. It is found that dayside ECH waves can efficiently pitch angle scatter ~300 eV to 10 keV electrons on timescales of a few hours to ~1 day, covering equatorial pitch angles from the loss cone to 45°. For higher energy electrons, the scattering tends to be less efficient and occurs over a narrower range of electron equatorial pitch angles. ECH wave induced scattering loss is found to be most intense for 300 eV to 2 keV electrons and the corresponding scattering rates can even approach the strong diffusion limit, resulting an almost fully filled loss cone. Our results demonstrate the crucial role

of ECH waves in the formation of dayside diffuse aurora which will improve the current understanding of the effects of resonant wave-particle interactions on the global distribution of electron diffuse auroral precipitation.

It is noted that the background magnetic field geometry, electron energy spectrum, ECH wave latitudinal coverage and spectral properties including the averaged amplitude and peak frequency on the dayside are all very different from that on the nightside (e.g., Lou et al., 2018; Ni et al., 2011b, 2017). All of them can affect the scattering efficiency of diffuse aurora electrons by ECH waves and the resultant precipitating electron fluxes. Thus, quantification of dayside ECH wave-driven electron precipitation is not a simple extension from the nightside. In our calculations of electron bounce-averaged scattering rates, we assume that the power spectral density of ECH waves and the plasma density remain constant along the magnetic field line following previous studies (e.g., Liang et al., 2011; Ni et al., 2011a, 2012). However, these parameters can vary considerably with the magnetic latitude and result in the changes in electron scattering rates. Therefore, it is necessary to perform a detailed analysis of the effects of the latitudinal variations of wave power spectral density and plasma density on the ECH wave-driven scattering of diffuse auroral electrons, which is left as a future work.

Previous studies have suggested that whistler-mode chorus waves also contribute to the production of dayside diffuse aurora (Ni et al., 2014; Nishimura et al., 2013; Shi et al., 2012, 2014). Chorus wave induced electron precipitation is found to be strongest from the nightside to dawn sectors over $4 < L < 6.5$ (Ma et al., 2020). Statistical observations show that both dayside ECH and chorus waves are mostly observed in the dawn MLT sector, which is consistent with the favorable occurrence of dayside diffuse aurora on the prenoon side (e.g., Frey et al., 2019; Newell et al., 2009). It will be of future interest to fully address the relative role of each of the above two wave modes in driving dayside diffuse auroral precipitation and their dependence on L-shell, MLT, and the level of geomagnetic activity. This requires further detailed quantitative evaluation of resonant scattering of plasma sheet electrons using statistical wave information.

Data Availability Statement

All MMS data used are available at (https://lasp.colorado.edu/mms/sdc/public/). The data used in this study and the numerical results can be obtained online from https://doi.org/10.6084/m9.figshare.13607609.v2.

Acknowledgments
The work was supported by the NSFC grants (42025404, 41904144, 41904143, 41974186, 41704162, 41674163, and 41574160), the B-type Strategic Priority Program of the Chinese Academy of Sciences (Grant No. XDB41000000), the pre-research projects on Civil Aerospace Technologies No. D020308, D020104, and D020303 funded by China National Space Administration, the China Postdoctoral Science Foundation (2020M672405 and 2019M662700) and the National Postdoctoral Program for Innovative Talents (BX20190252). Contributions by W. Tu were partially supported by NSF Grant AGS 1752736 and NASA Grant 80NSSC18K1284. We thank K. Liu and K. Min for their help with electron velocity distribution fitting.

References

Ashour-Abdalla, M., & Kennel, C. F. (1978). Nonconvective and convective electron cyclotron harmonic instabilities. *Journal of Geophysical Research*, *83*, 1531–1543. https://doi.org/10.1029/JA083iA04p01531

Burch, J. L., Moore, T. E., Torbert, R. B., & Giles, B. L. (2016). Magnetospheric multiscale overview and science objectives. *Space Science Reviews*, *199*(1–4), 5–21. https://doi.org/10.1007/s11214-015-0164-9

Cao, X., Ni, B., Liang, J., Xiang, Z., Wang, Q., Shi, R., et al. (2016). Resonant scattering of central plasma sheet protons by multiband EMIC waves and resultant proton loss timescales. *Journal of Geophysics Research: Space Physics*, *121*, 1219–1232. https://doi.org/10.1002/2015JA021933

Chaston, C. C., Bonnell, J. W., Kletzing, C. A., Hospodarsky, G. B., Wygant, J. R., & Smith, C. W. (2015). Broadband low-frequency electromagnetic waves in the inner magnetosphere. *Journal of Geophysical Research: Space Physics*, *120*, 8603–8615. https://doi.org/10.1002/2015JA021690

Chaston, C. C., Bonnell, J. W., Wygant, J. R., Reeves, G. D., Baker, D. N., & Melrose, D. B. (2018). Radiation belt "dropouts" and drift-bounce resonances in broadband electromagnetic waves. *Geophysical Research Letters*, *45*, 2128–2137. https://doi.org/10.1002/2017GL076362

Ergun, R. E., Tucker, S., Westfall, J., Goodrich, K. A., Malaspina, D. M., Summers, D., et al. (2016). The axial double probe and fields signal processing for the MMS mission. *Space Science Reviews*, *199*(1–4), 167–188. https://doi.org/10.1007/s11214-014-0115-x

Frey, H. U., Han, D., Kataoka, R., Lessard, M. R., Milan, S. E., Nishimura, Y., et al. (2019). Dayside aurora. *Space Science Reviews*, *215*, 51. https://doi.org/10.1007/s11214-019-0617-7

Han, D. S., Chen, X. C., Liu, J.-J., Qiu, Q., Keika, K., Hu, Z.-J., et al. (2015). An extensive survey of dayside diffuse aurora based on optical observations at Yellow River Station. *Journal of Geophysical Research: Space Physics*, *120*, 7447–7465. https://doi.org/10.1002/2015JA021699

Han, D. S., Li, J. X., Nishimura, Y., Lyons, L. R., Bortnik, J., Zhou, M., et al. (2017). Coordinated observations of two types of diffuse auroras near magnetic local noon by Magnetospheric Multiscale Mission and ground all-sky camera. *Geophysical Research Letters*, *44*, 8130–8139. https://doi.org/10.1002/2017GL074447

Hardy, D. A., Gussenhoven, M. S., & Holeman, E. (1985). A statistical model of auroral electron precipitation. *Journal of Geophysical Research*, *90*(A5), 4229–4248. https://doi.org/10.1029/JA090iA05p04229

Horne, R. B., & Thorne, R. M. (2000). Electron pitch angle diffusion by electrostatic electron cyclotron harmonic waves: The origin of pancake distributions. *Journal of Geophysical Research*, *105*(A3), 5391–5402. https://doi.org/10.1029/1999JA900447

Horne, R. B., Thorne, R. M., Meredith, N. P., & Anderson, R. R. (2003). Diffuse auroral electron scattering by electron cyclotron harmonic and whistler mode waves during an isolated substorm. *Journal of Geophysical Research*, *108*(A7), 1029. https://doi.org/10.1029/2002JA009736

Hu, Z.-J., Yang, H.-G., Han, D.-S., Huang, D.-H., Zhang, B.-C., Hu, H.-Q., & Liu, R.-Y. (2012). Dayside auroral emissions controlled by IMF: A survey for dayside auroral excitation at 557.7 and 630.0 nm in Ny-Ålesund, Svalbard. *Journal of Geophysical Research*, *117*, A02201. https://doi.org/10.1029/2011JA017188

Kennel, C. F. (1969). Consequences of a magnetospheric plasma. *Reviews of Geophysics and Space Physics*, *7*, 379–419. https://doi.org/10.1029/RG007i001p00379

Kennel, C. F., & Petschek, H. E. (1966). Limit on stably trapped particle fluxes. *Journal of Geophysical Research*, *71*, 1–28. https://doi.org/10.1029/JZ071i001p00001

Li, W., Bortnik, J., Thorne, R. M., & Angelopoulos, V. (2011). Global distribution of wave amplitudes and wave normal angles of chorus waves using THEMIS wave observations. *Journal of Geophysical Research*, *116*, A12205. https://doi.org/10.1029/2011JA017035

Li, W., Thorne, R. M., Angelopoulos, V., Bortnik, J., Cully, C. M., Ni, B., et al. (2009). Global distribution of whistler-mode chorus waves observed on the THEMIS spacecraft. *Geophysical Research Letters*, *36*, L09104. https://doi.org/10.1029/2009GL037595

Li, W., Thorne, R., Angelopoulos, V., Bonnell, J., McFadden, J., Carlson, C., & Auster, H. (2009). Evaluation of whistler-mode chorusintensification on the nightside during an injection event observed on the THEMIS spacecraft. *Journal of Geophysical Research*, *114*, A00C14. https://doi.org/10.1029/2008JA013554

Liang, J., Ni, B., Spanswick, E., Kubyshkina, M., Donovan, E. F., Uritsky, V. M., et al. (2011). Fast earthward flows, electron cyclotron harmonic waves, and diffuse auroras: Conjunctive observations and a synthesized scenario. *Journal of Geophysical Research*, *116*, A12220. https://doi.org/10.1029/2011JA017094

Lindqvist, P.-A., Olsson, G., Torbert, R. B., King, B., Granoff, M., Rau, D., et al. (2016). The spin-plane double probe electric field instrument for MMS. *Space Science Reviews*, *199*(1–4), 137–165. https://doi.org/10.1007/s11214-014-0116-9

Liu, X., Chen, L., & Xia, Z. (2020). The relation between electron cyclotron harmonic waves and plasmapause: Case and statistical studies. *Geophysical Research Letters*, *47*, e2020GL087365. https://doi.org/10.1029/2020GL087365

Lou, Y., Gu, X., Summers, D., Ni, B., Liu, K., Fu, S., et al. (2018). Statistical distributions of dayside ECH waves observed by MMS. *Geophysical Research Letters*, *45*, 12730–12738. https://doi.org/10.1029/2018GL080125

Lui, A. T. Y., Venkatesan, D., Anger, C. D., Akasofu, S.-I., Heikkila, W. J., Winningham, J. D., & Burrows, J. R. (1977). Simultaneous observations of particle precipitations and auroral emissions by the Isis 2 satellite in the 19–24 MLT sector. *Journal of Geophysical Research*, *82*, 2210–2226. https://doi.org/10.1029/JA082i016p02210

Ma, Q., Connor, H. K., Zhang, X. -J., Li, W., Shen, X. -C., Gillespie, D., et al. (2020). Global survey of plasma sheet electron precipitation due to whistler mode chorus waves in Earth's magnetosphere. *Geophysical Research Letters*, *47*, e2020GL088798. https://doi.org/10.1029/2020GL088798

Ma, Q., Mourenas, D., Artemyev, A., Li, W., Thorne, R. M., & Bortnik, J. (2016). Strong enhancement of 10–100 keV electron fluxes by combined effects of chorus waves and time domain structures. *Geophysical Research Letters*, *43*, 4683–4690. https://doi.org/10.1002/2016GL069125

Meng, C.-I., Mauk, B., & McIlwain, C. E. (1979). Electron precipitation of evening diffuse aurora and its conjugate electron fluxes near the magnetospheric equator. *Journal of Geophysical Research*, *84*, 2545–2558. https://doi.org/10.1029/JA084iA06p02545

Meredith, N. P., Horne, R. B., Thorne, R. M., & Anderson, R. R. (2009). Survey of upper band chorus and ECH waves: Implications for the diffuse aurora. *Journal of Geophysical Research*, *114*, A07218. https://doi.org/10.1029/2009JA014230

Mozer, F. S., Agapitov, O. V., Artemyev, A., Drake, J. F., Krasnoselskikh, V., Lejosne, S., & Vasko, I. (2015). Time domain structures: What and where they are, what they do, and how they are made. *Geophysical Research Letters*, *42*, 3627–3638. https://doi.org/10.1002/2015GL063946

Newell, P. T., Sotirelis, T., & Wing, S. (2009). Diffuse, monoenergetic, and broadband aurora: The global precipitation budget. *Journal of Geophysical Research*, *114*, A09207. https://doi.org/10.1029/2009JA014326

Ni, B., Bortnik, J., Nishimura, Y., Thorne, R. M., Li, W., Angelopoulos, V., et al. (2014). Chorus wave scattering responsible for the Earth's dayside diffuse auroral precipitation: A detailed case study. *Journal of Geophysical Research: Space Physics*, *119*, 897–908. https://doi.org/10.1002/2013JA019507

Ni, B., Cao, X., Zou, Z., Zhou, C., Gu, X., Bortnik, J., et al. (2015). Resonant scattering of outer zone relativistic electrons by multiband EMIC waves and resultant electron loss time scales. *Journal of Geophysical Research: Space Physics*, *120*, 7357–7373. https://doi.org/10.1002/2015JA021466

Ni, B., Gu, X., Fu, S., Xiang, Z., & Lou, Y. (2017). A statistical survey of electrostatic electron cyclotron harmonic waves based on THEMIS FFF wave data. *Journal of Geophysical Research: Space Physics*, *122*, 3342–3353. https://doi.org/10.1002/2016JA023433

Ni, B., Liang, J., Thorne, R. M., Angelopoulos, V., Horne, R. B., Kubyshkina, M., et al. (2012). Efficient diffuse auroral electron scattering by electrostatic electron cyclotron harmonic waves in the outer magnetosphere: A detailed case study. *Journal of Geophysical Research*, *117*, A01218. https://doi.org/10.1029/2011JA017095

Ni, B., Thorne, R. M., Horne, R. B., Meredith, N. P., Shprits, Y. Y., Chen, L., & Li, W. (2011a). Resonant scattering of plasma sheet electrons leading to diffuse auroral precipitation: 1. Evaluation for electrostatic electron cyclotron harmonic waves. *Journal of Geophysical Research*, *116*, A04218. https://doi.org/10.1029/2010JA016232

Ni, B., Thorne, R. M., Liang, J., Angelopoulos, V., Cully, C., Li, W., et al. (2011b). Global distribution of electrostatic electron cyclotron harmonic waves observed on THEMIS. *Geophysical Research Letters*, *38*, L17105. https://doi.org/10.1029/2011GL048793

Ni, B., Thorne, R. M., Meredith, N. P., Horne, R. B., & Shprits, Y. Y. (2011). Resonant scattering of plasma sheet electrons leading to diffuse auroral precipitation: 2. Evaluation for whistler mode chorus waves. *Journal of Geophysical Research*, *116*, A04219. https://doi.org/10.1029/2010JA016233

Ni, B., Thorne, R. M., Shprits, Y. Y., & Bortnik, J. (2008). Resonant scattering of plasma sheet electrons by whistler-mode chorus: Contributions to diffuse auroral precipitation. *Geophysical Research Letters*, *35*, L11106. https://doi.org/10.1029/2008GL034032

Ni, B., Thorne, R. M., Zhang, X., Bortnik, J., Pu, Z., Xie, L., et al. (2016). Origins of the Earth's diffuse auroral precipitation. *Space Science Reviews*, *200*(1–4), 205–259. https://doi.org/10.1007/s11214-016-0234-7

Nishimura, Y., Bortnik, J., Li, W., Thorne, R. M., Ni, B., Lyons, L. R., et al. (2013). Structures of dayside whistler-mode waves deduced from conjugate diffuse aurora. *Journal of Geophysical Research: Space Physics*, *118*, 664–673. https://doi.org/10.1029/2012ja018242

Orlova, K. G., & Shprits, Y. Y. (2010). Dependence of pitchangle scattering rates and loss timescales on the magnetic field model. *Geophysical Research Letters*, *37*, L05105. https://doi.org/10.1029/2009GL041639

Petrinec, S. M., Chenette, D. L., Mobilia, J., Rinaldi, M. A., & Imhof, W. L. (1999). Statistical X ray auroral emissions-pixie observations. *Geophysical Research Letters*, *26*(11), 1565–1568. https://doi.org/10.1029/1999GL900295

Pollock, C. J., Moore, T., Jacques, A., Burch, J., Gliese, U., Saito, Y., et al. (2016). Fast plasma investigation for magnetospheric multiscale. *Space Science Reviews*, *199*(1–4), 331–406. https://doi.org/10.1007/s11214-016-0245-4

Ronnmark, K. (1982). WHAMP: Waves in homogeneous, anisotropic, multicomponent plasmas, Kiruna Geophysical Institute, Report 179. Kiruna, Sweden: Kiruna Geophysical Institute.

Russell, C. T., Anderson, B. J., Baumjohann, W., Bromund, K. R., Dearborn, D., Fischer, D., et al. (2016). The magnetospheric multiscale magnetometers. *Space Science Reviews*, *199*(1–4), 189–256. https://doi.org/10.1007/s11214-014-0057-3

Sandholt, P. E., Denig, W. F., Farrugia, C. J., Lybekk, B., & Trondsen, E. (2002). Auroral structure at the cusp equatorward boundary: Relationship with the electron edge of low-latitude boundary layer precipitation. *Journal of Geophysical Research*, *107*(A9), 1235. https://doi.org/10.1029/2001JA005081

Shabansky, V. P. (1971). Some processes in the magnetosphere. *Space Science Reviews*, *12*, 299–418. https://doi.org/10.1007/BF00165511

Shi, R., Han, D., Ni, B., Hu, Z. J., Zhou, C., & Gu, X. (2012). Intensification of dayside diffuse auroral precipitation: Contribution of dayside whistler-mode chorus waves in realistic magnetic fields. *Annales Geophysicae*, *30*(9), 1297–1307. https://doi.org/10.5194/angeo-30-1297-2012

Shi, R., Hu, Z.-J., Ni, B., Han, D., Chen, X.-C., Zhou, C., & Gu, X. (2014). Modulation of the dayside diffuse auroral intensity by the solar wind dynamic pressure. *Journal of Geophysical Research: Space Physics*, *119*, 10092–10099. https://doi.org/10.1002/2014JA020180

Tao, X., Thorne, R. M., Li, W., Ni, B., Meredith, N. P., & Horne, R. B. (2011). Evolution of electron pitch angle distributions following injection from the plasma sheet. *Journal of Geophysical Research*, *116*, A04229. https://doi.org/10.1029/2010JA016245

Thorne, R. M., Ni, B., Tao, X., Horne, R. B., & Meredith, N. P. (2010). Scattering by chorus waves as the dominant cause of diffuse auroral precipitation. *Nature*, *467*, 943–946. https://doi.org/10.1038/nature09467

Torbert, R. B., Russell, C. T., Magnes, W., Ergun, R. E., Lindqvist, P. A., LeContel, O., et al. (2016). The FIELDS instrument suite on MMS: Scientific objectives, measurements, and data products. *Space Science Reviews*, *199*(1–4), 105–135. https://doi.org/10.1007/s11214-014-0109-8

Tsyganenko, N. A. (2002). A model of the near magnetosphere with a dawn-dusk asymmetry: 1. Mathematical structure. *Journal of Geophysical Research*, *107*(A8), 1179. https://doi.org/10.1029/2001JA000219

Tsyganenko, N. A., & Sitnov, M. I. (2005). Modeling the dynamics of the inner magnetosphere during strong geomagnetic storms. *Journal of Geophysical Research*, *110*, A03208. https://doi.org/10.1029/2004JA010798

Tsyganenko, N. A., & Stern, D. P. (1996). Modeling the global magnetic field of the large-scale Birkeland current systems. *Journal of Geophysical Research*, *101*, 27187–27198. https://doi.org/10.1029/96JA02735

Zhang, X., Angelopoulos, V., Ni, B., & Thorne, R. M. (2015). Predominance of ECH wave contribution to diffuse aurora in Earth's outer magnetosphere. *Journal of Geophysical Research: Space Physics*, *120*, 295–309. https://doi.org/10.1002/2014JA020455

Zhang, X., Angelopoulos, V., Ni, B., Thorne, R. M., & Horne, R. B. (2014). Extent of ECH wave emissions in the Earth's magnetotail. *Journal of Geophysical Research: Space Physics*, *119*, 5561–5574. https://doi.org/10.1002/2014JA019931

Zhang, X.-J., Chen, L., Artemyev, A. V., Angelopoulos, V., & Liu, X. (2019). Periodic excitation of chorus and ECH waves modulated by ultralow frequency compressions. *Journal of Geophysical Research: Space Physics*, *124*, 8535–8550. https://doi.org/10.1029/2019JA027201